JMEPEG
https://doi.org/10.1007/s11665-020-05097-x

1059-9495/$19.00

Residual Stress Characterization by X-Ray Diffraction and Correlation with Hardness in a Class D Railroad Wheel

A.B. Rezende, S.T. Fonseca, D.J. Minicucci, F.M. Fernandes, P.F.S. Farina, and P.R. Mei

(Submitted May 15, 2020; in revised form August 12, 2020)

This article focused on the microstructure characterization and residual stress measurements of the flange from classes D and C railway wheels (called 7D and 7C steel, respectively) to contribute with the residual stress level on new forged wheels flange area. A correlation with the hardness was conducted. The residual stress was measured in three points of the flange using the x-ray diffraction technique, and the microstructure characterization on SEM microscopy. We found the 7C steel has fine pearlite and ferrite microstructures, and 7D steel has degenerated pearlite and bainite microstructures. In the 7D steel, the compressive residual stress in the flange region was higher than in the 7C steel, which is related to the presence of bainite on the microstructure. There was a correlation between the hardness and residual stress value. The knowledge of the residual compression stress level is important for safety train wheels operation. The traction stress generated by the brake system on the wheel is attenuated by residual compression stress.

Keywords heavy haul, microalloyed steel, railway wheel, residual stress, x-ray analysis

1. Introduction

Railroad transportation has been widely used to move people and the economy of the countries over the years and has supported the development of many regions in the world (Ref 1). To increase the economic viability of the transport, researchers work to improve the transport safety, the weight capacity, and the train velocity (Ref 2, 3). In countries like Australia for example, the weight transported achieves 40 tons/axle (Ref 4). To support this weight increase, the development of new railway wheels is required. The Heavy Haul category (class D by Association of American Railroad-AAR) is the recent class of the railway wheels that have been developed to meet this demand. In these wheels, niobium, vanadium, and molybdenum are added in usual medium carbon steel, attaining higher toughness, mechanical, and wear resistance (Ref 5).

The high load on heavy haul operation induces high brake stress on the wheel, for this reason is so important to know and evaluate the residual compressive stress on class D wheels, in order to guarantee the safety operation for these wheels (Ref 6, 7). Besides, the flange supports the weight when the train passes by a curve stretch, and in this situation, higher tangential forces and contact stresses are detected (Ref 8). Residual stress is resulting from wheels manufacturing, and with control, it is beneficial to the wheel rolling contact fatigue (Ref 9). The techniques to measure the residual stresses in materials can be divided into destructive and nondestructive methods.

The advantage of nondestructive methods as x-ray diffraction is to be an effective and nondestructive process (Ref 10). In the technique, it is estimated the distortion in the crystal lattice by x-ray, and the residual stress is calculated assuming a linear elastic deformation of the crystal lattice (Ref 11). As a disadvantage, the waves penetrate a certain distance in the sample (on average over a few microns under the surface) and depend on the anode, material, and angle of incidence (Ref 12). Besides, complete measurements of residual stress by x-ray diffraction are restricted in the literature for railway wheels in the function of the measured restrictions.

The residual stress distribution in the forged railway wheels is influenced by the manufacturing process because of the last thermal treatment of quenching (Ref 13). This heat treatment provides compressive residual stress below the tread (Ref 14) and the depth of the heat treatment is a function of the hardenability of the steel. According to Rezende et al. (Ref 15), the addition of some alloy elements acts to decrease the start temperature of martensite formation and may influence the results of the quenching process.

We propose in this research a microstructure characterization and the measurement of residual stress using the x-ray diffraction method in flange from a new class D wheel and comparing with commercial class C wheel.

2. Materials and Methods

2.1 Samples

The specimens were obtained from the class C and new class D forged railroad wheels (denominated 7C and 7D steel, respectively). The chemical composition measured by optical spectrometry (ARL 3460 OES, Thermo Scientific) is presented in Table 1. The main difference between the chemical elements

A.B. Rezende, S.T. Fonseca, F.M. Fernandes, P.F.S. Farina, and **P.R. Mei**, Faculty of Mechanical Engineering, University of Campinas, Campinas, SP 13083-860, Brazil; and **D.J. Minicucci**, DJ Consulting, Botucatu, SP, Brazil. Contact e-mail: andreibavaresco@gmail.com.

Published online: 08 September 2020

of 7C and 7D steels is the addition of the percentual of chromium, molybdenum, and niobium. The final heat treatment for the two wheels was austenitization at 890 °C, quenching and, tempering at 500 °C.

The two original wheel samples were transversely cut in the flange region of the wheel (Fig. 1). It is worth mentioning that stress relaxation occurs due to the cutting process. However, due to the impossibility of measuring large parts by x-ray diffraction, the measurement in small pieces can comprise a good approximation to the real residual stress according to Prevey (Ref 16) and Takahashi et al. (Ref 9). The surface preparation of the specimens was grinding and electro-polishing.

2.2 Microstructure Characterization

The microstructure characterization was carried out from scanning electron microscopy (SEM) (EVO MA 15, Zeiss-UNICAMP). Microhardness was measured with a durometer (FV 800, Future Tech.), applying 0.5 kgf for 15 s five times in the same locations of the residual stress measurements. The x-ray diffraction measurements were performed in Brazilian Nanotechnology National Laboratory (CNPEM/LNNano) installations using a diffractometer "Panalitical X'pert Pro" with the following parameters: Co Kα radiation, tube voltage, and current 40 (kV) and 45 (mA), respectively, 2θ range from 40° to 130°.

2.3 Residual Stress X-ray Diffraction

The residual stress measurements by x-ray diffraction are based on the distortion of the crystal lattice. The presence of residual stress changes the interplanar distances of the material due to the deformation in the crystal lattice and modifies the diffraction peak normally found in the material free of stress (Ref 11, 12).

The $\sin^2\psi$ method was used on residual stress measurements. Assuming the low penetration (a few microns) of x-rays, the plane stress state is considered zero (Ref 17). The equation that governing the method is given in Eq 1 (Ref 11, 16). Rotation phi (φ) and tilt psi (ψ) angle of the x-ray diffractometer goniometer governing the biaxial stress tensor σ_φ. So, for each angle ψ (psi) is achieved a respective interplanar distance d_ψ. It is recommended to use 2θ angle greater than 120° to higher precision (Ref 16)

$$\sigma_\varphi = \left(\frac{d_\psi - d_0}{d_0}\right)\left(\frac{1+v}{E}\right)\left(\frac{1}{\sin^2\psi}\right) \quad \text{(Eq 1)}$$

The lattice spacing d_ψ is a linear function of $\sin^2\psi$, and to multiples ψ tilts. From the d-spacing values and ψ tilts, the least-square line is obtained. Supposing the unstressed d_o is known and using material constants from the literature E (Young module) and ν (poison coefficient), the residual stress is calculated by the slope of the least-squares line (Ref 16-18). The software "Panalitical X'Pert Stress" was used to fit the least-square line concerning the $\sin^2$ ψ method and the parameters of Table 2.

The measurements were performed in Brazilian Nanotechnology National Laboratory (LNNanno/CNPEM) installations using the same diffractometer previously mentioned. Three points equally spaced at transversal cutting samples of the flange (Fig. 1) were measured in each sample (7C and 7D steel). These points were selected in function of the flange geometry and the size of the irradiated area promoted by the diffractometer. On account of the symmetry between the three components directions, the measurements were performed in a hoop direction (Ref 19).

Table 1 Chemical composition of the samples (wt.%)

Sample	C	Si	Mn	Cr	Cu + V	Mo + Nb Nb
7C Steel	0.778	0.342	0.809	0.200	0.207	0.041
7D Steel	0.725	0.274	0.880	0.352	0.200	0.142

3. Results and Discussion

The microstructure of the 7C and 7D steel was obtained from SEM analysis and are illustrated in Fig. 2 and 3. In the 7C steel, the hardness was 357 ± 7 HV and the microstructure was mostly composed of fine pearlite and some sites of grain boundary ferrite. The microstructure is coherent due to the manufactured process and the elements present in its composition, likewise the study by Fonseca et al. (Ref 5). The microstructure in the 7D steel presented hardness of 400 ± 20 HV, being mostly composed of degenerated pearlite, some sites of grain boundary ferrite, and bainite (Ref 20). The microstructure was similar to railway wheel material studied by Minicucci et al. (Ref 4). These authors used steel with similar content of molybdenum and niobium in the chemical composition. According to Rezende et al. (Ref 15), the addition of these alloy elements in steel changes the kinetics of the transformation during the steel cooling. Thus, in the same position for 7C and 7D steel, we observe different microstructure.

The 2θ x-ray measurement confirmed the phases that compose the two steel. The diffraction peaks collected represent the crystalline planes for ferrite crystalline structure, and austenite phase was not detected (Ref 21). The austenitic phase

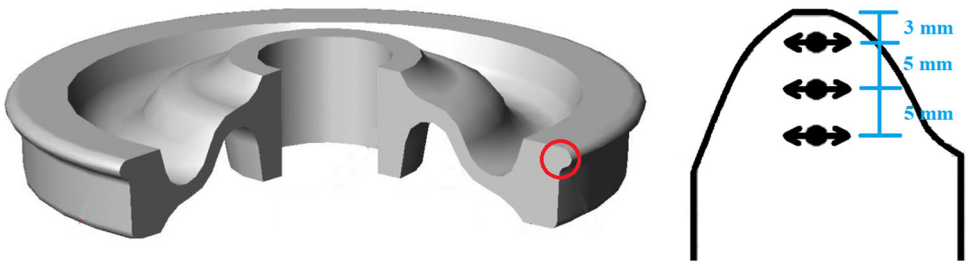

Fig. 1 Representation of a sample in the railway wheel and measure points in the flange region indicating hoop direction

Table 2 Parameters of x-ray measurements to residual stress calculation

Method	Convergent beam method
X-ray characteristic	Cr-Kα
K-β filter	Vanadium
Diffraction angle 2θ (deg)	152.2 to 159.1
Sin^2 ψ (Steps)	11
Sin^2 ψ (Range)	− 0.175 to 0.175
Counting time (s)	5.35
Generator tension (kV)	30
Generator current (mA)	55
Irradiated area (mm^2)	4.8
E (Young Module)	207 GPa
ν (Poisson Coefficient)	0.3
Fitting method	Profile shape function-Pearson II

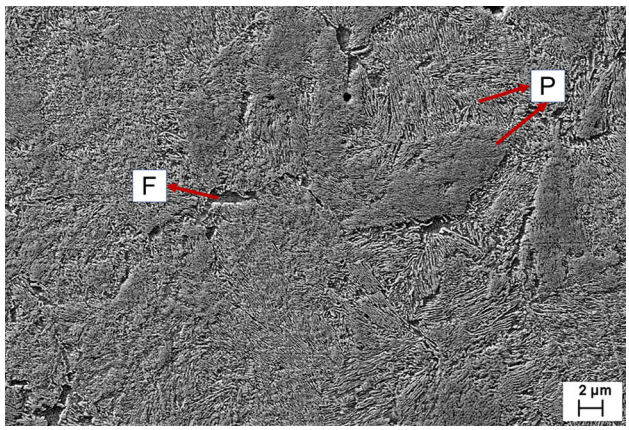

Fig. 2 Scanning Electrons Microscopic (SEM) analysis of 7C steel. (P-pearlite), (F-grain boundary ferrite). (Etching Nital 2%)

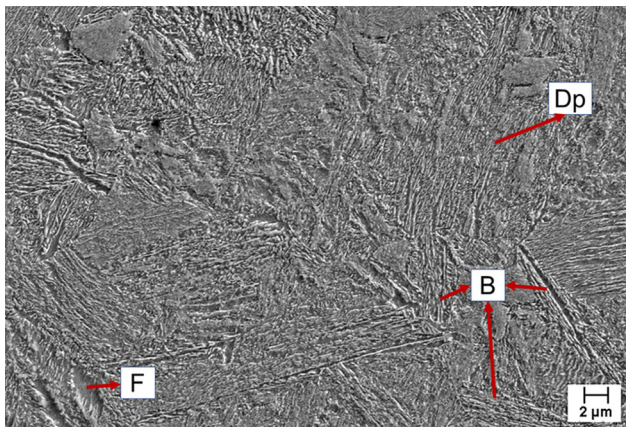

Fig. 3 Scanning Electrons Microscopic (SEM) analysis of 7D steel (F-grain boundary ferrite), (Dp-degenerated pearlite), (B-bainite). (Etching Nital 2%)

present in the wheel would be transformed to martensite under operation due to the high contact pressure between the rail and wheel. This martensite transformation is no desirable because of the possibility of cracks nucleation by Rolling Contact Fatigue (Ref 22, 23).

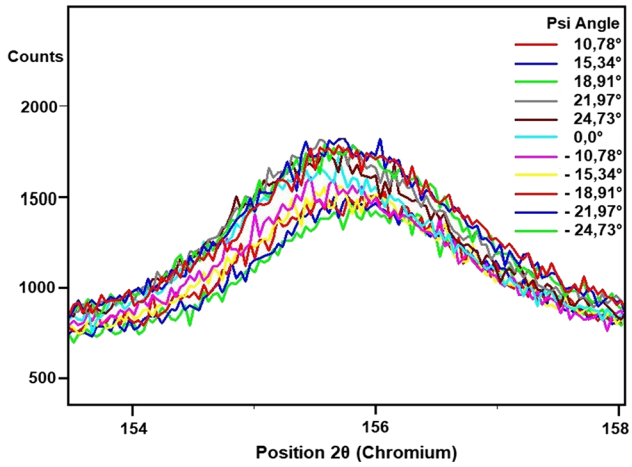

Fig. 4 Example of diffraction curves obtained for each point in the sample

In residual measurements, each point returned 11 diffraction curves from 152.2 to 159.1° diffraction angles (θ) as exemplified in Fig. 4. Using software X'Pert Stress, the proprieties of the material were inserted and the profile shape function (Pearson II) was used to fit the least-square line. The residual stress value was obtained applying the $\sin^2\psi$ method for each psi (ψ) angle.

In Fig. 5, we present the residual stress medium value for 7C and 7D steel. The residual stresses for both steels were compressive (negative value), and the higher medium values were 237 and 415 MPa to 7C and 7D steel, respectively. The results for 7C steel are within the range of residual stress presented by Brunel et al., (Ref 24). The 7D steel presented compressive residual stress values higher than the literature and could be associated with the difference in the chemical composition that changed the characteristics of the microstructure.

The difference between the residual stress module values of 7D and 7C steel was related to the alloy elements addition in 7D steel (molybdenum, niobium, and chromium) that changed the kinetic of material transformation (Ref 25, 26). The impact was the change in the microstructure of fine pearlite into degenerated pearlite and bainite which increased the hardness as illustrated in Fig. 6. The presence of bainite on microstructure in 7D steel increases the number of dislocations (Ref 27) which increment the value of compressive residual stress (Ref 28).

Figure 6 presents a decrease in the compressive residual stress as the analyzed depth is increased, following the tendency exhibited in studies such as Goo and Seo (Ref 29), Brunel et al. (Ref 24). As the depth increase, the hardness also reduces evidencing a correlation between the residual stress and the hardness. This behavior is verified because the region near the surface suffered more influence of the heat treatment in previous cycles (Ref 7, 30).

On the reported of Fig. 7, there was a correlation between the hardness and the residual stress value. This correlation followed the tendency found by Frankel et al. (Ref 31) and Takakuwa et al. (Ref 32) in measurements of hardness and residual stress. Bocciarelli and Maier (Ref 33) affirmed that compressive residual stress difficult the penetration of indenter which collaborate to increase the hardness value.

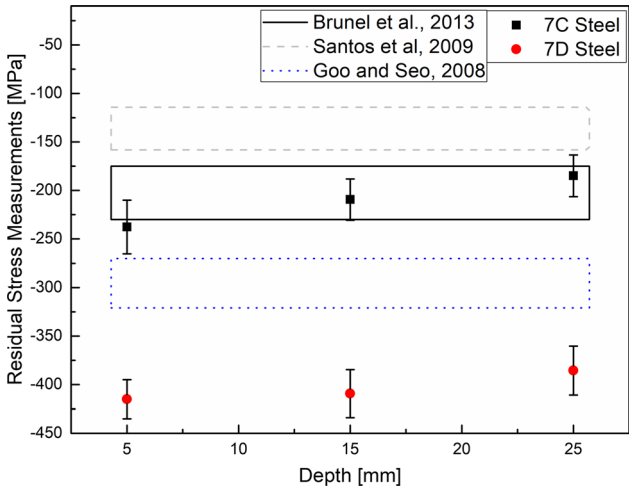

Fig. 5 Residual stress measurements for 7C and 7D steel and compared with literature values

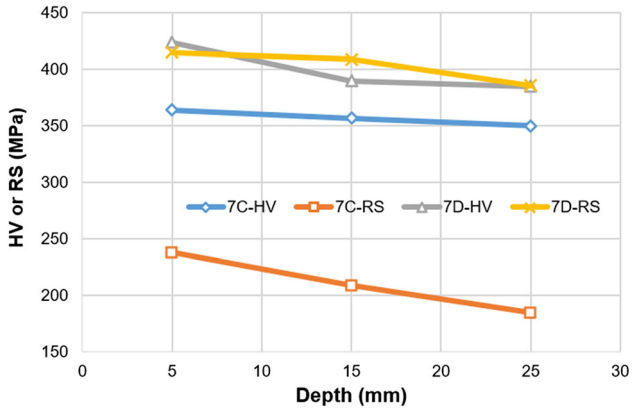

Fig. 6 Compressive residual stress module (RS) and hardness (HV) versus the measurement depth

According to the literature, the compressive residual stress is favorable to prolong the appearance of the rolling contact fatigue cracks on wheels being a factor to extend their life cycle (Ref 34, 35). As the class D wheels operate with a higher load applied, the increase of residual stress will be beneficial and will prolong the life in service (Ref 7). Besides, the higher residual stress would be beneficial to prevent problems with the high load induced by high brake stress on the wheels. There was not observed martensite in the microstructure either unusual inclusions.

Concerning the correlation between hardness and residual stress, these results support the possibility of estimate the residual stress in other wheels by hardness measurements. However, it is worth mentioning that the estimative must carefully be done only for forged wheels with heat treatment temperatures like those used in this work.

4. Conclusion

The microstructure characterization and the measurement of residual stress using the x-ray diffraction method for classes C and D of railway wheels in the flange region were proposed.

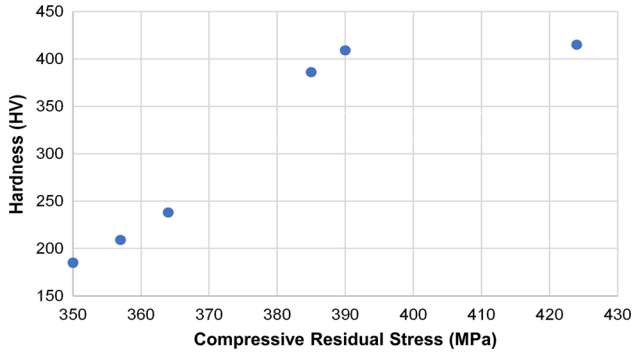

Fig. 7 Correlation between compressive residual stress and hardness (HV)

Based on the experimental results and analysis, the following conclusion can be defined.

We verified that both studied steels presented compressive residual stress. The residual stress module values of 7D steel were higher than the 7C steel values and the data achieved in the literature for class C forged railway wheels.

On microstructural characterization, 7C steel featured fine pearlite as the main microstructure and sites of ferrite. On the other hand, 7D steel featured degenerated pearlite as the dominant microstructure with sites of ferrite and bainite. The changes in the microstructure provided a higher hardness for 7D steel.

The residual stress presented a correlation with the hardness for 7C and 7D steel. As the depth increase the hardness and the residual stress value decrease. This correlation was a novelty because there was no similar investigation in the literature yet. As the hardness measures are more accessible than residual stress measures, checking this measure can be easier.

Acknowledgments

The authors thank research supported by LNNano-Brazilian Nanotechnology National Laboratory, CNPEM/MCTIC-Metals Characterization and Processing Laboratory and, the Brazilian National Council for Scientific and Technological Development (CNPQ).

References

1. M. Faccoli, A. Ghidini, C. Petrogalli, M. Faccoli, M. Lancini, and A. Mazzù, Effect of Desert Sand on Wear and Rolling Contact Fatigue Behavior of Various Railway Wheel Steels, *Wear*, Elsevier B.V., 2017, **396-397** (2017), p 146–161
2. S.R. Lewis, R. Lewis, G. Evans, and L.E. Buckley-Johnstone, Assessment of Railway Curve Lubricant Performance Using a Twin-Disc Tester, *Wear*, 2014, **314**(1–2), p 205–212
3. M. Clarke, Wheel Rolling Contact Fatigue and Rim Defects Investigation to Further Knowledge of the Causes of RCF and to Determine Control Measures, *Rail Saf. Stand. Board*, 2008, p 1–20
4. D.J. Minicucci, S.T. Fonseca, R.L.V. Boas, H. Goldenstein, and P.R. Mei, Development of Niobium Microalloyed Steel for Railway Wheel with Pearlitic Bainitic Microstructure, *Mater. Res.*, 2019, **22**(6), p 8
5. S.T. Fonseca, A. Sinatora, A.J. Ramirez, D.J. Minicucci, C.R. Afonso, and P.R. Mei, Effects of Vanadium on the Continuous Cooling Transformation of 0.7%C Steel for Railway Wheels, *Defect Diffus. Forum*, 2016, **367**, p 60–67

6. D. José Minicuci, A.A. Santos, M.H. Andrino, and F.C. Santos, Stress Evaluation of Railroad Forged Wheels by Ultrasonic Testing, *J. Test. Eval.*, 2007, **35**(1), p 17
7. D.H. Stone and S.M. Cummings, Effect of Residual Stress, Temperature and Adhesion on Wheel Surface Fatigue Cracking, *American Society of Mechanical Engineers, Rail Transportation Division (Publication) RTD*, 2009, p 157–165
8. H. Ishida, T. Miyamoto, E. Maebashi, H. Doi, K. Iida, and A. Furukawa, Safety Assessment for Flange Climb Derailment of Trains Running at Low Speeds on Sharp Curves, *Q. Rep. RTRI*, 2006, **47**(2), p 65–71
9. S. Takahashi, T. Kato, H. Suzuki, and T. Sasaki, Residual Stress Evaluation of Railway Wheels by X-ray Diffraction and Finite Element Method, *Adv. Mater. Res.*, 2010, **89–91**, p 545–550
10. K. Moussaoui, S. Segonds, W. Rubio, and M. Mousseigne, Studying the Measurement by X-ray Diffraction of Residual Stresses in Ti6Al4V Titanium Alloy, *Mater. Sci. Eng. A*, 2016, **667**, p 340–348
11. M.E. Fitzpatrick, a T. Fry, P. Holdway, F. a Kandil, J. Shackleton, and L. Suominen, Determination of Residual Stresses by x-Ray Diffraction-Issue 2, *Meas. Good Pract. Guid.*, 2005, **52**(2), p 1–68
12. R.B. Ceglias, J.M. Alves, N. Robbers, D. Cajueiro, S.B. Diniz, and L.P. Brandao, Residual Stress Evaluation by x-Ray Diffraction and Hole-Drilling in an API, 5L X70 Steel Pipe Bent by Hot Induction s i N, *Mater. Res.*, 2016, **19**(5), p 1176–1179
13. "Association of American Railroad" AAR M-107, Manual of Standards and Recommended Practices, Section G, 2011, p 180
14. P.B. Molyneux-Berry, A.J. Bevan, S.Y. Zhang, and S. Kabra, Residual Stress in Wheels: Comparison of Neutron Diffraction and Ultrasonic Methods with Trends in RCF, *Civil-Comput. Proc.*, 2014, **104**, p 1–17
15. A.B. Rezende, F.M. Fernandes, S.T. Fonseca, P.F.S. Farina, H.Goldenstein, and P.R. Mei, Effect of Alloy Elements in Time Temperature Transformation Diagrams of Railway Wheels, *Defect Diffus. Forum*, (Athens), 2020, **400**, p 11–20
16. P.S. Prevéy, X-Ray Diffraction Residual Stress Techniques, *Met. Handbook. 10. Met. Park*, 1986, (513), p 380–392
17. F. Yang, J.Q. Jiang, Y. Wang, C. Ma, F. Fang, K.L. Zhao, and W. Li, Residual Stress in Pearlitic Steel Rods during Progressively Cold Drawing Measured by X-ray Diffraction, *Mater. Lett.*, 2008, **62**(15), p 2219–2221
18. O. Anderoglu, Residual Stress Measurement Using X-ray Diffraction, M.S. thesis in Mechanical Engineering Texas A&M University, 2004
19. R.H.F. Melo, M.A. Dos Santos, and T.M. Maciel, Avaliação Do Campo de Tensões Residuais Por Difração de Raios-X Utilizando o Método Do Sen2ψ Em Revestimentos Metálicos Do Aço Inoxidável S308-l. (Evaluation of the Residual Stresses Field by X-ray Diffraction Using the Sen2ψ Method in S308-L Stainless, *Soldag. e Inspeção*, 2013, **18**(1), p 50-56 (portuguese)
20. F.G. Caballero, M.J. Santofimia, C. García-Mateo, and C.G. de Andrés, Time-Temperature-Transformation Diagram within the Bainitic Temperature Range in a Medium Carbon Steel, *Mater. Trans.*, 2004, **45**(12), p 3272–3281
21. A. Taniyama, T. Takayama, M. Arai, and T. Hamada, Structure Analysis of Ferrite in Deformed Pearlitic Steel by Means of X-ray Diffraction Method with Synchrotron Radiation, *Scr. Mater.*, 2004, **51**, p 53–58
22. A. Ekberg, B. Åkesson, and E. Kabo, Wheel/Rail Rolling Contact Fatigue - Probe, *Predict, Prevent, Wear, Elsevier*, 2014, **314**(1–2), p 2–12
23. Q. Li, X. Huang, and W. Huang, Fatigue Property and Microstructure Deformation Behavior of Multiphase Microstructure in a Medium-Carbon Bainite Steel under Rolling Contact Condition, *Int. J. Fatigue*, Elsevier, 2019, **125**(24), p 381–393
24. F. Brunel, J.F. Brunel, P. Dufrénoy, and F. Demilly, Prediction of the Initial Residual Stresses in Railway Wheels Induced by Manufacturing, *J. Therm. Stress.*, 2013, **36**(1), p 37–55
25. A. Fadel and D. Gli̇, Influence of Cr, Mn and Mo Addition on Structure and Properties of V Microalloyed Medium Carbon Steels, *J. Mater. Sci. Technol.*, 2012, **28**(11), p 1053–1058
26. D. Gallina, Finite Element Prediction of Crack Formation Induced by Quenching in a Forged Valve, *Eng. Fail. Anal.*, 2011, **18**(8), p 2250–2259
27. C. Goulas, A. Kumar, M.-G. Mecozzi, F.M. Castro-Cerda, M. Herbig, R.H. Petrov, and J. Sietsma, Atomic-Scale Investigations of Isothermally Formed Bainite Microstructures in 51CrV4 Spring Steel, *Mater. Charact.*, 2019, **152**, p 67–75
28. S. Chang, Y.S. Pyun, and A. Amanov, Wear Enhancement of Wheel-Rail Interaction by Ultrasonic Nanocrystalline Surface Modification Technique, *Materials (Basel).*, 2017, **10**(2), p 12
29. B.C. Goo and J.W. Seo, Finite Element Analysis of the Rolling Contact Fatigue Life of Railcar Wheels, *Mater. Sci. Forum*, 2008, **575–578**, p 1461–1466
30. É.F. Santos, D.J. Minicucci, R.S. Barbosa, and L. Padovese, *Inspection of Forged Railway Wheels by a Magnetic Barkhausen Noise Non-Destructive Testing Method to Evaluate Residual Stresses of Manufacturing*, Chengdu, International Wheelset Congress, 2016, p 1–4
31. J. Frankel, A. Abbate, and W. Scholz, The Effect of Residual Stresses on Hardness Measurements, *Exp. Mech.*, 1993, **33**(2), p 164–168
32. O. Takakuwa, Y. Kawaragi, and H. Soyama, Estimation of the Yield Stress of Stainless Steel from the Vickers Hardness Taking Account of the Residual Stress, *J. Surf. Eng. Mater. Adv. Technol.*, 2013, **03**(04), p 262–268. https://doi.org/10.4236/jsemat.2013.34035
33. M. Bocciarelli and G. Maier, Indentation and Imprint Mapping Method for Identification of Residual Stresses, *Comput. Mater. Sci.*, 2007, **39**, p 381–392
34. J. Gordon and B. Perlman, Estimation of Residual Stresses in Railroad Commuter Car Wheels Following Manufacture, *International Mechanical Engineering Congress*, (Anaheim), 2003, p 91
35. D.J. Minicucci, Avaliação de Tensões Por Ultra-Som No Aro de Rodas Ferroviárias Forjadas Novas–Classe C. (Stress Evaluation by Ultrasound in Rim of the New-Class C Forged Railway Wheels), M.S. thesis, University of Campinas, p. 199, 2003